

B. Haftmann  
F.-J. Debbeler  
H. Gielen

Messerschmitt-Bölkow-Blohm GmbH  
Transport Aircraft Group  
Bremen, Germany

### Abstract

A semi-empirical method is described which was applied to predict the preflight drag of the A310 and the A300-600 for take-off, one engine conditions.

The first part of the present paper is concerned with wind tunnel models and tests basically designed to obtain aerodynamic performances at low speeds, i.e. drag and maximum lift. In addition, special measurements with turbine powered simulators (TPS) are described which were performed to investigate the effect of installed engines on 2nd segment climb drag.

The correction of tunnel results to full scale aircraft data is subject of the next part. A simple scaling rule is shown covering the effect of Reynolds number on lift, pitching moment and drag. The quality of this rule is demonstrated by a comparison of scaled results with corresponding model data obtained in a pressurized wind tunnel.

The third part of the paper compares flight test results with corresponding predictions for several take-off configurations. It is demonstrated that with the model/test philosophy and the scaling method described the predictions agree with the flight test data within a range of  $\pm 1\%$  of overall drag.

### I. Introduction

The take-off performances of transport aircraft are usually defined by second segment climb conditions where for twin engine jets a climb rate of 2.4% with one engine inoperating has to be demonstrated. Fig. 1 bottom picture shows this take-off procedure. The second segment starts with "under-

carriage in" and ends 400 ft over ground. During this period the minimum climb rate of 2.4% has to be demonstrated with an aircraft speed not less than 20% over stall speed. The aircraft drag at these conditions can be split into two parts

- the symmetrical portion of the basic configuration
- the asymmetrical portion which includes one engine windmill drag and the trim drag due to rudder/aileron deflection

This paper concentrates on the prediction method applied to obtain the symmetrical drag portion.

As shown in the left hand picture of Fig. 1 the most important contributions are the lift dependent drag with approx. 80% and the shape drag with approx. 18%. Both portions are  $R_N$  dependent which effect is subject of this paper.

### II. Basic Windtunnel Tests

#### II.-1 Complete model measurements

#### General Test Requirements

To establish the basic drag level, tunnel tests are needed which provide data of high accuracy and repeatability.

Hence, low tunnel flow turbulence, high balance accuracy, model suspensions of low interference and careful model design are required. Within Airbus Industrie mainly three tunnels are used with priority to get low speed performances. These are the pressurized facilities Fauga F1, test section 4.5m X 3.5m and RAE 5m and the atmospheric tunnel DNW with a test section of 6m X 8m. With the method described in this paper it is of less importance which test Reynolds number is chosen if the flow behaviour up to  $C_{L1.2Vs}$  is as expected

for the aircraft. This means that flow separations which do not exist at full scale Reynolds numbers have to be avoided either by partial model modifications or by tests at higher Reynolds numbers. In any case before starting performance tests one has to check the flow behaviour around the model.

#### Model Arrangements and Accuracy

Fig. 2 and 3 shows the A310 and the A300-600 model arrangements in the DNW. Suspension is a single sting combined with an internal strain gage balance. Compared with a three strut suspension, also shown in the figure, which usually is used in the pressurized tunnels, the single sting provides less interference but the accuracy of internal balances are usually less than the accuracy of external ones. The main difficulty with internal balances of the size we are talking about, are inhomogeneous temperature effects which are different between installed and laboratory conditions and which are therefore not easy to compensate. In a very close cooperation with the DNW these problems have been minimized and we are now at a long time repeatability of about  $\pm 5$  drag counts which is less than  $\pm 0.5\%$  of the total second segment climb drag.

#### Model Configuration

The basic tests are carried out with the model in tail-off configuration. As shown in Fig. 4 all parts of the model except the wing are provided with carborundum strips to fix the location of the laminar/turbulent boundary layer transition. This enables the shape drag calculation under consideration of an exact known laminar portion. The strips should be positioned just behind the pressure peaks and a transition check with china clay or another technique should be carried out before starting force measurements. The table shows the strip positions chosen for A310 and A300-600 models being tested in the DNW.

fuselage	60 mm	from the nose
pod	28 mm	from L.E.
pylon	16 mm	perpendicular to L.E.
vertical tail	5%	chord

#### Transition Strip Positions on A300 and A310 Models

Because of the nature of pressure distribution on the wing with slats deployed a natural transition at or near the leading edge occurs which makes an artificial promoter unnecessary.

#### Engine Representation

The engines are generally represented by through flow nacelles. As shown in Fig. 4 the CF6-80A is designed as a single body skirted nacelle extended to the end of the hot gas nozzle. However, this simple design cannot be applied in general, especially if the fan exit plane is close to the wing leading edge. In those cases it is better to design a double body nacelle where the interference between fan exit and wing becomes more representative with special respect to maximum lift investigations. The nacelles are designed to provide a mass flow ratio representing the "flight idle" condition of the real engine at Mach = 0.2 and 5000 ft altitude. Fig. 5 illustrates this design point within the range of most important engine conditions at low speeds. It can be seen that both A310 engine types, i.e. GE and P&W agree well in absolute values and their development versus Mach number. However, the range of mass flow ratios between windmill and maximum take-off power is comparably large. The sketches beside the curves give an impression of the corresponding different stream tubes and it is obvious that the mass flow ratio will influence the overall forces and moments of the aircraft. Tests to obtain these effects will be described later.

#### Test Conditions

As mentioned before, the Reynolds number does not necessarily influence the final accuracy of the drag assessment, it should however not be less than  $2 \times 10^6$ . Mach number should be 0.2 or less. In any case it is important that the maximum lift does not include Mach effects. Later on it will be shown that the  $R_N$  corrections to be applied are depending on the ratio of model/full scale maximum lift which explains that others than  $R_N$ -effects would falsify the result. The importance of representative maximum lift measurements compared with the expected flight value leads also to the choice of the flight idle condition for the through flow nacelle design, because this is the engine condition for demonstrating minimum speeds in flight.

## 1.1.-2 Engine Interference Measurements

### General Introduction

Coming back to Fig. 5 and the different flow field around the engines at second segment climb conditions. The range of mass flow ratio to be covered is windmill on one side and maximum take-off power on the other limit. The shaded area indicates aircraft speed which lies between Mach = 0.2 and 0.3. For the engine in maximum power condition the free stream tube area is between 20% and 100% bigger than the inlet area. It is obvious that the simulation of such flow field requires special test techniques, i.e. models with powered nacelles.

Fig. 6 shows a selection of possible concepts. The most simple one is the "blown nacelle" which uses a faired intake and where the jet stream is simulated by pressurized air fed into the nacelle from external sources. This technique needs additional tests to determine the intake flow effect and is only practicable if intake and exit flow do not interfere with each other.

A step forward compared with the "blown nacelle" technique is the "ejector nacelle". This solution makes it possible to simulate intake and exit flow simultaneous, however, with limited accuracy. The main problems with this technique are that the intake mass flow of the ejector reaches only 50 to 60% of the real engine mass flow and that the nozzle exit flow is of high turbulence which leads to a relatively quick jet decay with corresponding interference effects, not comparable with the real engine behaviour.

The most promising technique is the "turbine powered simulator" TPS which originally was used only for high speed investigations. Since 1980 MBB have installed this technique to check engine interference effects also at low speeds. The DNW followed 1982 with the possibility to test complete models with two TPS running in different conditions.

### TPS Measurements

Fig. 7 shows an A310 half model of 1/16 scale in the MBB Bremen windtunnel. The model is fitted with a 5" TPS unit faced to represent CF6-80A geometry. Drive air is guided via a precise force-free airbridge through the balance into the TPS. The

drive air operates a turbine which moves the fan. The advantage of this technique is a precise representation of geometry, pressure ratio and mass flow of the fan jet.

Different from the real engine are the intake mass flow, temperature and velocity of the gas generator jet efflux. However, because the hot gas part on the gross thrust of modern high bypass engines is small and the hot jet is rounded by the fan jet, the incorrect simulation of this part is assumed to have negligible effects. By this reason the similarity is concentrated on the fan jet where the velocity ratio

$$\frac{V_E}{V_\infty} = \frac{\text{fan jet exit velocity}}{\text{free stream velocity}}$$

is assumed to be the standard parameter.

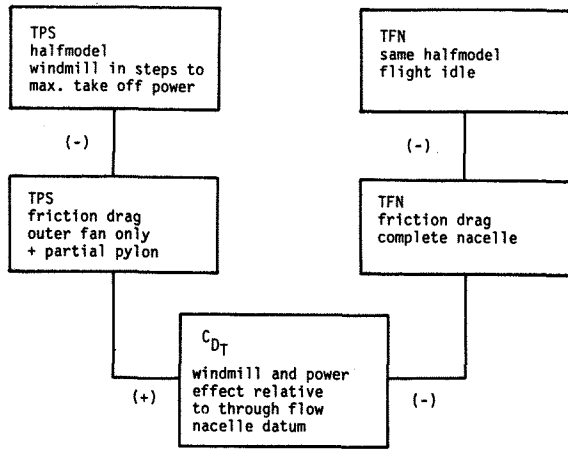
Attention has to be paid to the TPS intake area. Here the mass flow is reduced by the gas generator part where the drive air is guided direct into the turbine and therefore not passed through the intake. The reduction is approximately 14% for engines with bypass ratio of 6 : 1. Our experience is that a corresponding reduction of the TPS intake area supplied by a reshaped outer contour results in the best approach to the flow behaviour of the real engine.

One severe problem arises from the fact that the thrust at low speed conditions is higher than the aircraft drag. It is therefore very important to determine the TPS thrust with extremely high accuracy. For this purpose MBB use the calibration tank shown in Fig. 8. The balance developed for this tank has an accuracy of  $\pm 0.1\%$ , but it is of same importance to have control units and electronic equipment to a comparable high standard. It was useful in this connection for instance to take the same wire arrangement for calibration and tunnel test.

### Evaluation of Engine Interference Drag

There are, of course, different philosophies and definitions to get the engine interference effects. MBB uses the following approach:

Test and Analysis Procedure



TPS thrust components in lift and drag direction are corrected in this approach, just as the internal drag portion of the through flow nacelle which can either be determined by theoretical calculations or extra calibration tests. The TPS thrust definition includes internal losses, the friction drag of the hot gas nozzle and the pylon part which is covered by the fan jet. This definition is agreed with engine manufacturer. The  $\Delta C_D$  values will be determined at constant lift values.

III. Drag Scaling Procedures

III.-1 General

After establishing the basic drag level "tail off" by the tunnel tests described before, the following corrections have to be applied to obtain final full scale values :

- correction of shape drag due to Reynolds number
- correction of lift dependent drag, lift and pitching moments due to Reynolds number
- correction of thrust effects
- trimming
- miscellaneous

III.-2 Correction of shape drag

The lift independent minimum drag correction is simply the difference between model and full scale shape drags, calculated for the respective Reynolds number :

$$\Delta C_{D_0(R_N)} = C_{D_0(A/C R_N)} - C_{D_0(Model R_N)}$$

The  $C_{D_0}$  values in this formula represent the sum of individual calculated shape drags for each part of the model or the aircraft, i.e. wing, fuselage, tails etc.. As usual the shape drags are defined to be flat plate skin friction multiplied by a shape factor:

$$C_{D_0} = C_f \cdot \frac{S_W}{S_R} \cdot \lambda$$

Skin Friction Drag

The variation of skin friction with Reynolds number was subject of extensive experimental investigations up to the 60s. Several authors, for instance Prandtl-Schlichting, Karman-Schoenherr, Schultz-Grunow etc., have developed empirical formulae derived from these data which differ slightly in their results. For the range of interest  $2 \times 10^6 < R_N < 30 \times 10^6$  the maximum deviation of the  $R_N$  dependent drag described by these formulae is less than 0,25% of the total symmetrical drag. So, in contrast to the high speed case where this deviation might become more important because the cruise drag coefficient is much lower, there is no special preference for one or the other equation in the low speed take off case. Nevertheless, for the prediction of the fully turbulent part MBB uses Prandtl-Schlichting, given by :

$$C_{f(T)} = \frac{0,455}{(\log R_{N_C})^{2.58}}$$

where  $R_{N_C}$  is the Reynolds number based on local chord. Compressibility effects will not be considered in this speed range.

The laminar part due to the smaller Reynolds number at windtunnel model condition up to transition-strips is given by the Blasius equation :

$$C_{f(L)} = \frac{1,328}{\sqrt{R_{N_C}}}$$

For the aircraft, fully turbulent boundary layer is assumed on all parts .

Wing and Tailplanes

The geometry of the wing in high lift configuration is defined in Fig. 9 which also illustrates a typical wing thickness distribution. Basis is the clean wing, flaps and flaps retracted for which the shape drag is given by :

$$C_{DoW} \cdot S_{Ref.} = 4b \int_{\eta_1}^1 C_f(\eta) \cdot \lambda(\eta) \cdot c(\eta) \cdot d\eta$$

where

- $S_{Ref.}$  is the reference area
- $b$  is the half span of the exposed wing respectively those of the tails, flaps and slats
- $C_f(\eta)$  is the skin friction drag dependent on spanwise position
- $\lambda(\eta)$  is the shape factor dependent on spanwise position (Fig. 10)
- $C(\eta)$  is the wing chord

Shape factors for several wing profiles are published in ESDU papers. A selection is given in Fig. 10 which can be applied on typical modern wing and tailplane sections. Because these shape factors are valid for the unswept case, the sweep-effect corrected value becomes:

$$\lambda = (\bar{\lambda} - 1) \cos^2 \varphi_{50} + 1$$

where

$\varphi_{50}$  is the sweep angle of the 50% chord line.

The wing shape drag in high lift configuration, flaps and flaps deployed, is assumed to be the clean wing value multiplied by the wetted area factor, flaps and slat shape drags added :

$$C_{D_{oHigh Lift}} = C_{D_{oW}} \cdot \frac{S_{WRest}}{S_{Wclean}} + C_{D_{oF}} + C_{D_{oS}}$$

where

- $S_{WRest}$  is the shaded area shown in Fig. 9,
- $C_{D_{oF}}, C_{D_{oS}}$  are the shape drags of flaps and slats.

### Flaps and Slats

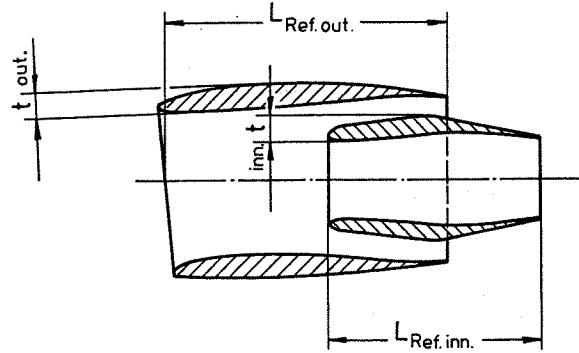
Shape drags has to be calculated in the same way as for the wing. However, the determination of the shape factor (unswept) can be simplified to :

$$\bar{\lambda} = 1 + 2.7 (t/c) + 100 (t/c)^4$$

Geometrical definitions see Fig. 9.

### Pods

The definition of the model through flow nacelle geometry is shown below.



Definition of Engine Dimensions

For model nacelles it is recommended to calculate the wetted area on basis of a mean diameter for each body. The shape factor, can be determined by the equation :

$$\lambda = 1 + 2,7 (t/L_{Ref.}) + 100 (t/L_{Ref.})^4$$

The pod shape drag becomes :

$$C_{D_{op}} = C_f \cdot \frac{S_W}{S_{Ref}} \cdot \lambda \quad (\text{model})$$

For the aircraft only the outer part of the fan cowl contributes to the aircraft drag, hence the wetted area should be determined on the basis of the outer diameter and the drag has to be calculated without application of a shape factor :

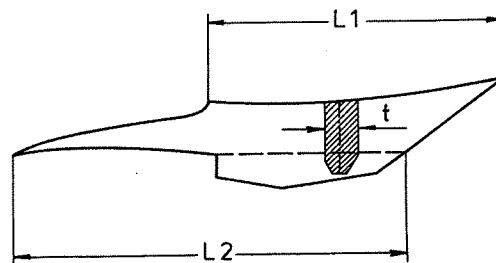
$$C_{D_{oP}} = C_f \cdot \frac{S_W}{S_{Ref}} \quad (\text{aircraft})$$

where

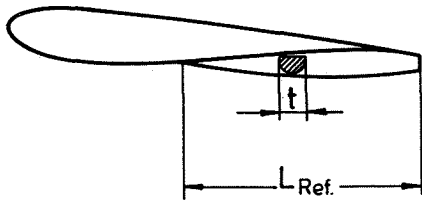
$S_W$  is the wetted area of the fan cowl outer contour.

### Pylon and Flap Track Fairings

Typical pylon and fairing geometries are shown below.



Definition of Pylon Dimensions



Definition of Fairing Dimensions

The Reynolds number to determine the skin friction coefficients is based on  $L_{Ref}$ , which, in case of the pylon, is a mixture of  $L_1$  and  $L_2$ . In any case the wetted areas are calculated to be twice of the projection area. For the shape drag same formulae can be applied as for the model pods.

#### Fuselage

In case of the A310 and A300-600 the fuselage contributes with more than 30% on the total shape drag of the aircraft. It therefore plays the most important part within the  $C_{D_0}$  corrections. The calculation is similar to the other aircraft components. With the shape factor shown in Fig. 11 the fuselage drag becomes :

$$C_{D_0} = C_f \cdot \frac{S_W}{S_{Ref}} \cdot \lambda$$

where the Reynolds number is referred to the complete fuselage length.

#### Summary Chapter II.-2

A summary of the calculated A310 shape drags is shown in Fig. 12. This picture demonstrates that in general the aircraft component drag levels are of same order of magnitude as the wetted areas. Exceptions are fuselage and slats. The fuselage contributes with approximately 45% on the total wetted area but the drag portion is only 32% which indicates that, although the A310 fuselage is attributed to the wide body family, the shape factor is relatively small compared with other components. Against that, the slats produce round 15% of drag by a wetted area contribution of approximately 5%. With this the slats produce after fuse-

lage and wing the highest shape drag of all aircraft components. Fig. 13 shows the calculated A310 shape drag versus Reynolds number for the aircraft and the model which was tested in the DNW. The discontinuous function is due to the difference in the pod drags where for the model inner and outer part have to be accounted for, whereas at the aircraft only the fan cowl outer portion contributes to the aircraft drag. Flight reference and model test Reynolds number are marked in the figure. The difference between the calculated drags at these conditions is the shape drag correction to be applied on the model results. The amount is 96 drag counts which corresponds to 7% of the total aircraft drag at a typical take-off configuration.

### III.-3 Correction of Lift Dependent Drag, Lift and Pitching Moments due to Reynolds number

#### General

A general assumption to arrive at the correct drag level is that the model flow behaviour is close to the expected aircraft behaviour. This requirement defines a minimum test Reynolds number where no flow separation occurs in the lift range of interest (up to  $C_{L_{1.2V_{smin}}}$ ) and where the maximum lift is controlled by same type and position of separated flow as on the aircraft. If one compares such tunnel measurements with flight tests or with tunnel results obtained at higher Reynolds numbers, on principle the higher Reynolds number results show

- higher maximum lift at higher angles
- similar but later beginning nonlinearities
- stretched polar shapes.

It has been found that this behaviour can be regulated. Following the assumption that the viscous effect on lift for any Reynolds number is proportional to the respective maximum lift, the general scaling law becomes :

$$C_{L(A/C)} = \frac{C_{Lmax(A/C)}}{C_{Lmax(M)}} \cdot C_{L(M)}$$

where (A/C) is standing for "aircraft" or any other reference - Reynolds number and (M) for "model" Reynolds number and test result. The unknown aircraft maximum lift has to be determined either by a combination of tunnel data and flight

test results of existing aircraft or other prediction methods. Fig. 14 shows the principle of the applied corrections.

### Correction of Lift

As already mentioned the lift transposition to flight is

$$C_{L(A/C)} = \frac{C_{Lmax(A/C)}}{C_{Lmax(M)}} \cdot C_{L(M)}$$

The lift belongs to an aircraft angle of incidence which becomes

$$\alpha(A/C) = \frac{C_{Lmax(A/C)}}{C_{Lmax(M)}} (\alpha(M) - \alpha_o(M)) + \alpha_o(M)$$

This equation can be derived by the assumption that zero lift angle  $\alpha_o$  and the lift curve slope in its linear region is identical for model and aircraft conditions. Of course, this assumption is limited to moderate flap settings where the initial aerodynamic load is comparably small.

### Correction of Pitching Moments

Due to the change in maximum lift and in maximum angle of incidence the pitching moments also have to be corrected although the effect on trim drag is very small. With the assumption that zero pitching moment  $C_{M_o}$  and the slope versus lift in its linear region is identical for model and aircraft, the corrected value becomes

$$C_{M(A/C)} = \frac{C_{Lmax(A/C)}}{C_{Lmax(M)}} (C_{M(M)} - C_{M_o(M)}) + C_{M_o(M)}$$

which is equivalent to the formula for the  $\alpha$  correction.

### Correction of Lift Dependent Drag

The lift region of interest for which the second segment climb drag should be properly defined lies between  $C_L(1.4V_{smin})$  and  $C_L(1.2V_{smin})$ . This corresponds to lift values of 60 to 80% of the maximum lift (lg). The drag in this region can be sufficiently described by the equation

$$C_D = C_{D_o} + \frac{K}{\pi \cdot A} \cdot C_L^2$$

where the lift dependent portion

$K/(\pi \cdot A) \cdot C_L^2$  consists of the induced drag

$K/(\pi \cdot A) \cdot C_L^2$  and an additional Reynolds number dependent part  $C_{DC}$  which is subject of the correction. In most of the cases it is sufficient to work with the ideal induced drag ( $K_1 = 1$ ) so that finally the Reynolds number dependent drag portion is defined by

$$C_{DC} = C_{D(M)} - C_{D_o(M)} - \frac{C_L^2(M)}{\pi \cdot A}$$

This portion, obtained from model tests, is assumed to be same for the aircraft at lift values of same proportional distance to the maximum lift value. That means

$$C_{DC} = f \left( \frac{C_L}{C_{Lmax}} \right)$$

is assumed to be independent from Reynolds number as indicated in Fig. 14 bottom left sketch. The final aircraft drag, untrimmed without tail, is then defined by :

$$C_{D(A/C)} = C_{DC} + \Delta C_{D_o(RN)} + \frac{C_L^2(A/C)}{\pi \cdot A}$$

where

$C_{D(A/C)}$  is the aircraft drag at  $C_L(A/C)$

$C_{DC}$  defined above is the drag portion at  $C_L(M)$ , which is  $C_L(A/C) \cdot \frac{C_{Lmax(M)}}{C_{Lmax(A/C)}}$

$\Delta C_{D_o}$  is the correction of shape drag due to Reynolds number as defined in chapter II-2

The lift dependent drag correction term at constant lift can then be expressed by the equation :

$$\Delta C_{Di(RN)} = (K(M) - 1) \left[ \left( \frac{C_{Lmax(M)}}{C_{Lmax(A/C)}} \right)^2 - 1 \right] \cdot \frac{C_L^2}{\pi \cdot A}$$

For typical take-off lift value and a test Reynolds number of  $2 \times 10^6$  this part of correction results in 2 - 3% of the total aircraft drag.

## III.-4 Residual Drag Corrections

### Trimming

The scaled wing/fuselage configuration has to be trimmed to the forward centre of gravity position and for a reference gross thrust coefficient  $C_{TG}$ . The consideration of thrust is limited to the pitching moment coefficients, whereas the thrust contribution to the aircraft lift will be regarded with the field length calculation.

The drag increment due to trim at constant aircraft lift consists of the tail drag due to tail lift and the higher wing/body drag due to the lift increase which is necessary to overcome the lift loss on the tail for balancing the wing/body pitching moment. Referred to the tail area the tail drag portion becomes :

$$C_{D_T} = \underbrace{\frac{K_T}{\pi \cdot A_T} (C_{L_T} - C_{L_{OT}})^2 \cos \epsilon}_{\text{Tail induced drag}} + \underbrace{C_{L_T} \sin \epsilon}_{\text{Tail thrust}}$$

Herein the tail lift follows from the aircraft's wing/body pitching moment including thrust contribution in the course of which it is recommendable to correct the wing/body pitching moments first to zero gross thrust (see next chapter) to make the coefficients independent from the designed mass flow ratio of the model nacelle. Then, assuming that the moments are referred to 25% AMC, the tail lift to trim is

$$C_{L_T} = \frac{\textcircled{1} CM(A/C) + (X_{c.g.}/AMC - 0.25) \cdot \textcircled{2} CL(A/C) + \textcircled{3} Z_A}{\left( \frac{LT - X_{c.g.}}{AMC} + 0.25 \right) \cdot \frac{S_T}{S_{Ref}}}$$

- ① is the wing/body pitching moment corrected to zero gross thrust
- ② regards the centre of gravity position
- ③ is the thrust contribution (see next chapter).

Because the so defined trim lift is referred to the tail force system and to the tail area the final contribution to the trimmed aircraft lift becomes :

$$\Delta C_{L_{T(A/C)}} = C_{L_T} \cdot \frac{S_T}{S_{Ref}} \cdot \cos \epsilon$$

and the drag

$$\Delta C_{D_T(A/C)} = C_{D_T} \cdot \frac{S_T}{S_{Ref}}$$

The total increment from wing/body to the trimmed aircraft drag at given lift is approximately :

$$\Delta C_{D_{Trim}} \approx C_{D_{OT}} + \textcircled{2} \Delta C_{D_T(A/C)} - 2 \cdot \frac{K(A/C)}{\pi \cdot A(A/C)} \textcircled{3} \Delta C_{L_T(A/C)} \cdot C_{L(A/C)}$$

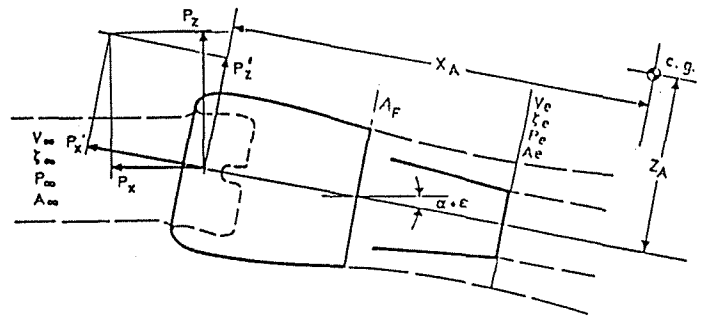
where

- ① is the tail shape drag including interference fuselage/tail

- ② is the tail lift dependent drag portion to trim
- ③ is the wing/body drag contribution caused by increasing the angle of incidence to overcome the trim lift loss

### Thrust effect

Normally the thrust is not part of the aerodynamic coefficients. An exception is the data basis for performance calculations where the thrust contribution on pitching moment is part of the trimming procedure. It therefore influences indirect the aircraft drag polar.



Defintion of Engine Geometry and Notation

On basis of the above definitions and after some simplifications the total engine contribution on the aircraft pitching moment can be derived to :

$$\Delta C_{M_E} = \frac{\textcircled{1} FG - FR}{q \cdot S_{Ref}} \cdot \frac{Z_A}{MAC} + \left( \frac{FR}{q \cdot S_{Ref}} + 2 \frac{A_e}{S_{Ref}} \right) \frac{X_A}{MAC} \cdot \alpha'$$

where

- ① is the net thrust portion
- ② is due to the change of inlet momentum direction
- ③ is due to the change of "apparent mass flow" momentum direction

On basis of this formula special cases can be derived, such as for the model through flow nacelle where in a first approach the net thrust can be assumed to be zero. Then the model pod contribution becomes :

$$\Delta C_{M_P} = \left[ \frac{FR}{q \cdot S_{Ref}} + 2 \frac{A_e}{S_{Ref}} \right] \frac{X_A}{MAC} \cdot \alpha'$$



This means that the pure aerodynamic portion for model and full scale engine is identical if geometry and mass flow ratio are equivalent. The effect of divergent mass flow ratios from the reference condition have to be taken from TPS measurements as mentioned at the beginning.

In most of the cases it is profitable to correct the model pitching moments to zero gross thrust which is :

$$\Delta \Delta C_{M_p} = -2 \left( \frac{A_\infty}{A_{Ref.}} \right) \cdot \frac{A_{Ref.}}{S_{Ref.}} \cdot \frac{Z_A}{MAC}$$

where

$\frac{A_\infty}{A_{Ref.}}$  is the designed nacelle mass flow ratio (flight idle).

If the model based pitching moments have been corrected in that way the full scale thrust contribution becomes :

$$\Delta C_{M_E (A/C)} = C_{T_G} \cdot \frac{Z_A}{MAC}$$

where

$C_{T_G}$  is the gross thrust coefficient of the running engines ( $C_{T_G} = \frac{F_G}{q \cdot S_{Ref.}}$ )

#### Parasitics

The parasitic drag contributes to the total take-off drag with approximately 1%. It covers those portions which are not represented on the model, i.e. the effect of gaps, steps, roughnesses, antennae etc.. Usually, the computation follows for a typical cruise Mach number but the result will be adopted for low speeds, too. Here, only a short description about the applied methods shall be given

The calculation of parasitic drag items is based largely on semi-empirical methods and in the literature there exists a wide spectrum of experimental data for excrescences. The most important calculation methods can be summarized into two main groups :

Excrescences such as steps, gaps, holes, etc. on the aircraft surface which are small compared with the local boundary layer thickness ( $h/\delta < 0.1$ ). For these the method of Wieghardt [10] gives the best data reduction :

$$\frac{C_D}{C_f} = f \left( \frac{U_\tau \cdot h}{\nu}; M_\delta \right)$$

where

$\frac{U_\tau \cdot h}{\nu}$  is the local Reynolds number based on the step height and the local friction velocity

$M_\delta$  is the local Mach number

Details are given also in Ref. [11] and [12]

For relatively large excrescences such as antennae, drainmasts, lights and other bodies which project far into the boundary layer or through it ( $h > \delta$ ) the calculation method after Hoerner [13] has been applied where an "independent drag" coefficient is defined which is referred to the frontal area and an effective dynamic pressure :

$$\bar{C}_D = \frac{D}{q_{eff.} S_f} = f \left( \frac{\bar{u} h}{\nu}; M_\delta \right)$$

where the effective dynamic pressure has to be derived from a boundary layer computation.

#### IV. Comparison of Scaled with Measured Drags

##### IV.-1 Justification of the Method by

##### Tunnel Measurements

Fig. 15 shows results of an A310 test campaign which was carried out at a very early development stage in the pressurized NLR high speed tunnel. Plotted are lift, pitching moment and drag coefficients measured at Mach = 0.2 and different Reynolds numbers for a typical take-off configuration with slats and flaps deployed. The picture demonstrates the typical effect of increased Reynolds number, i.e. higher maximum lift, similar but later beginning nonlinearities and lower drag.

Starting from the low Reynolds number test ( $R_N = 1.7 \times 10^6$ ) the scaling method has been applied to estimate coefficients for the higher test Reynolds number. The result is shown by the dashed lines which demonstrate fairly good agreement with the corresponding measurements. The diagrams of most interest are placed on the bottom of the figure. On the right hand side the total drags are shown where the scaled drag includes  $C_{D_0}$  and  $C_D = f(C_L)$  changes. In this

case the complete correction sums up to approx. 70 drag counts which overestimates the measured effect due to Reynolds number by approx. 10 counts.

To the left the normalized drag is shown where the  $C_D$  difference is eliminated. This picture demonstrates how the lift dependent correction operates. In this case the agreement of the normalization with respect to maximum lift is excellent. However, other investigations on various projects, which were carried out since that time, show that the scatter of this correction part is in the order of  $\pm 0,5\%$  for a range of Reynolds numbers between  $2 \times 10^6$  and  $6 \times 10^6$ .

#### IV.-2 Comparison with Flight Test Results

Performance flight tests have been carried out by Airbus Industrie in the usual manner with individually calibrated engines. The second segment flights were done with one engine in windmill condition as well as with both engines operating symmetrically. The drag has been calculated via a personified thrust deck and analysed by application of a regression method. The results are shown in Fig. 16 for the A310 and in Fig. 17 for the A300-600. Both diagrams contain L/D values versus  $C_L$  for three take-off configurations and for landing where the marked area represents a band width of  $\pm 1\%$  L/D around the mean. For comparison in Fig. 16 the scaled drags based on RAE (triangles) and DNW (circles) tunnel tests are shown. The agreement is good. Only for configuration I which is the slat out/flap in case the mean of the scaled results lie outside the band for a small  $C_L$  region. The scaled tunnel results themselves differ less than 2% from each other. The A300-600 is aerodynamically very similar to the A300-B4. The most important differences, which nevertheless have only small effects at low speeds, are the flap system change from tabbed to simple fowler flap and the wing tip fence. Therefore, only limited low speed tunnel tests are available for this aircraft. The scaled drag shown in Fig. 17 is based on DNW tests. Here the agreement is of less quality but still acceptable. The biggest divergence occurs for configuration II which represents flaps settings of  $8^\circ$ . It seems in this case that the basic tunnel results are of less accuracy. The maximum divergence is in the

order of 2% L/D outside the band. This example might demonstrate that confirmation measurements in different tunnels and with various models are necessary to establish a well proven prediction basis.

#### V. Conclusions

This survey has presented some of the main features of the drag scaling method used by MBB to predict the second segment climb drag of transport aircraft. In particular, the wind tunnel testing philosophy, the degree of engine simulation and the corrections due to the effect of Reynolds number has been outlined. To demonstrate the overall validity of this method tunnel and flight test results obtained with the aircraft A310 and A300-600 have been shown in comparison with the scaled values. The principle conclusions to be noted are :

1. A careful model/tunnel concept is necessary to provide the basic drag and maximum lift level with the required accuracy. In particular, it has to be ensured that the model flow behaviour on the wing in high lift configuration is close to the expected aircraft flow pattern. Laminar portions of the model boundary layer have to be limited by an optimized fixation.
2. It is recommended to determine the engine installation effects by using TPS units. However, because of the complexity of this technique the investigation should be limited to measure differences to a well defined engine reference condition which is "flight idle" in this case and which is represented on the basic performance model by a corresponding designed "through flow" nacelle.
3. The quality of the determined corrections depend mainly on the accuracy of the calculated differences between model and aircraft, i.e. shape drags and maximum lifts. Therefore the absolute levels are not so significant. This fact allows some simplifications in particular for the calculation of wetted areas.

4. It has been demonstrated that the introduced [12] ESDU  
 drag estimation method is useful. A comparison  
 with flight test results of two different  
 transport aircraft show acceptable agreements.

References

- [1] Paterson, J.H., MacWilkinson, D.G. and  
 Blackerby, W.T.  
 A Survey of Drag Prediction Techniques  
 applicable to Subsonic and Transonic  
 Aircraft Design.
- [2] RAeS Data sheets, Wings 02.04.02, 03.
- [3] RAeS Data Sheets, Bodies 02.04.01, 02.
- [4] Schlichting, H.  
 Boundary Layer Theory  
 Fourth Ed., MacGraw-Hill Book Co.,  
 Inc., 1960
- [5] USAF Stability and Control DATCOM,  
 Section 4.4.1, 1969  
 Wing-Body Combinations at Angle of Attack
- [6] Schultz-Grunow, F.  
 New Frictional Resistance Law for  
 Smooth Plates.  
 NACA TM 986, 1941
- [7] Schoenherr, K.E.  
 Resistance of Flat Surfaces Moving Through  
 a Fluid.  
 Trans. Soc. Naval Architects and Marine  
 Engineers, Vol. 40, 1932, pp. 279-313
- [8] Abbott, I.R., Von Doenhoff, A.E.,  
 Stivers, L.S.  
 Summary of Airfoil Data  
 NACA Rept. 824, 1945
- [9] Winter, K.G.  
 A Program of Tests on the Drag of  
 Excrescences Proposed for the  
 8 ft X 8 ft Wind Tunnel and a Brief  
 Analysis of some Previous Measurements.  
 1967
- [10] Wieghardt, K.  
 Increase in Turbulent Skin Friction caused  
 by Surface Irregularities.  
 MAP R&T No. 103, Translation of FB 1563,  
 ZWB 1942, 1946
- [11] Gaudet, L. Johnson, P.  
 Measurements of Drag of Excrescences  
 Immersed in Turbulent Boundary Layers at  
 Mach Numbers between 0,2 and 2,8.  
 RAE TR 71 181, 1971
- [12] ESDU  
 Drag of Two-Dimensional Steps and Ridges  
 Immersed in a Turbulent Boundary Layer  
 for Mach Numbers up to 3.0.  
 Engineering Sciences Data Nr. 75 031, 1975
- [13] Hoerner, S.F.  
 Fluid Dynamic Drag  
 Published by the author.
- [14] Ewald, B. and Smyth, R.  
 The Role and Implementation of Different  
 Nacelle/Engine Simulation Concepts for Wind-  
 Tunnel Testing in Research and Development  
 Work on Transport Aircraft.  
 AGARD, Fluid Dynamics Panel Meeting  
 Toulouse, France, 1981
- [15] Krenz, G.  
 Transonic Wing Design for Transport Aircraft  
 Presentation for the AIAA "Advancing Tech-  
 nology", Williamsburg, Virginia, USA,  
 March 26-28, 1979
- [16] Klevenhusen, K.D., Jakob, H. and Struck, H.  
 Calculation of Wing-Body-Nacelle Interference  
 in Subsonic and Transonic Potential Flow  
 AGARD, Fluid Dynamics Panel Meeting  
 Toulouse, France, 11.-14. May, 1981
- [17] Rohde, J.  
 Voruntersuchungen am Prinzipmodell der Trieb-  
 werks-Durchfluß-Simulation für das ZKP-  
 Großmodell.  
 VFW-Kurzbericht Ef-826, ZKP-Flügelsektion-  
 Bericht Nr. 38
- [18] Burgsmüller, W.  
 Grundlagen zur Triebwerkssimulation mittels  
 TPS im Windkanal.  
 VFW-Kurzbericht Ef-915, ZKP-IFAS-Bericht  
 Nr. 5

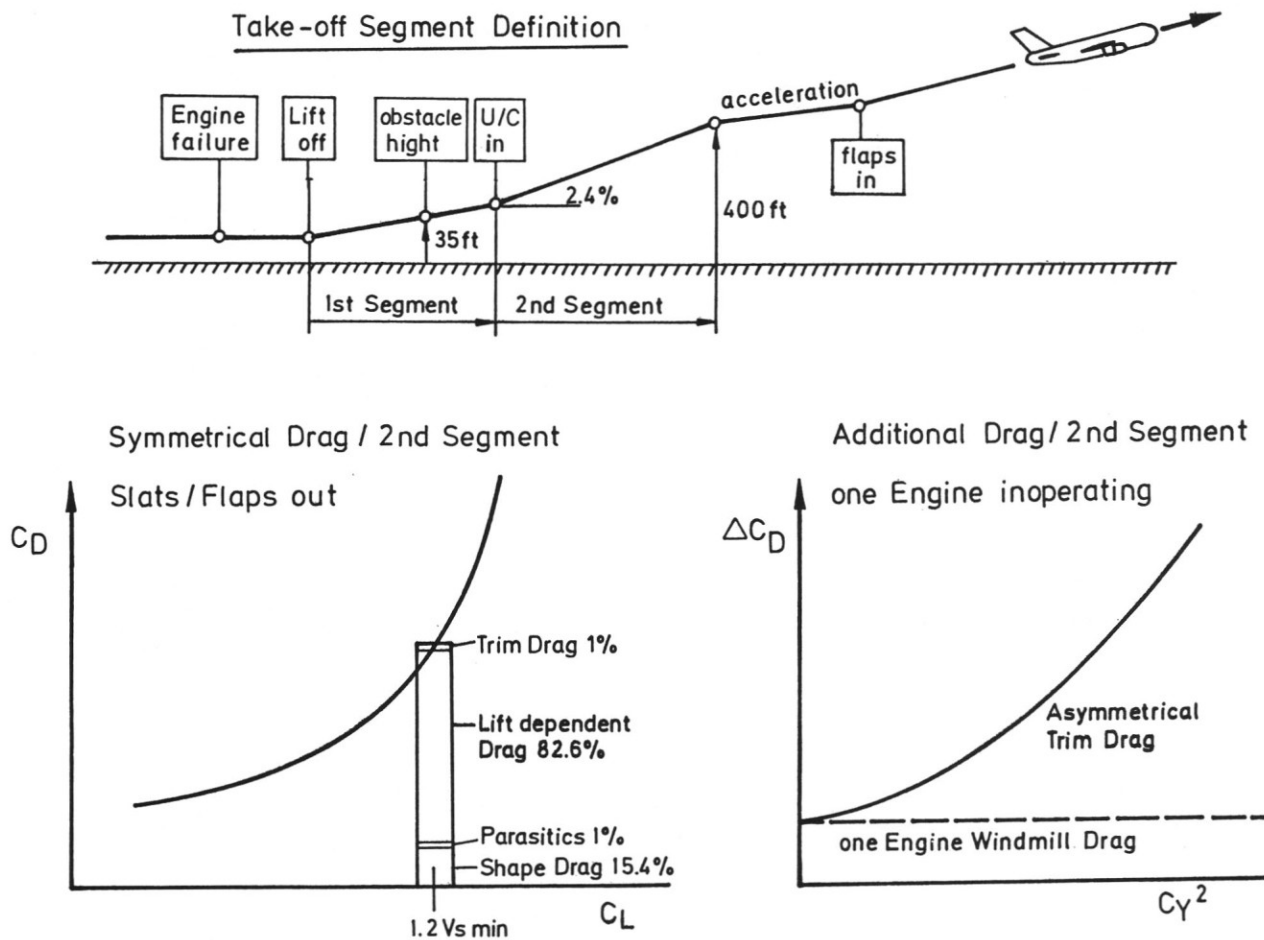


FIG. 1 Take-Off Segment Definitions and Drag Portions



FIG. 2 A310 Model Arrangement in the DNW

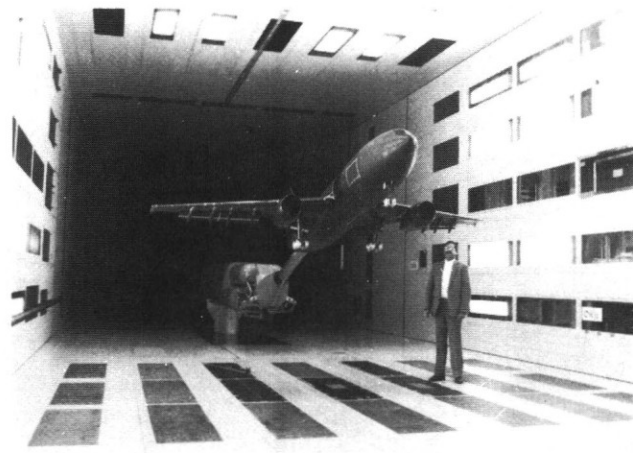


FIG. 3 A300-600 Model Arrangement in the DNW

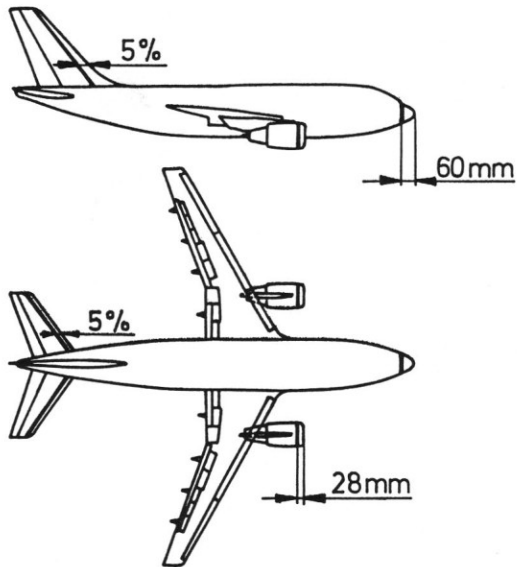


FIG. 4 Transition Fixing on A310 Models

	Task	Engine Conditions
Performance	• Drag	max. Power / Windmill
	• max.Lift	Flight Idle
Handling	• Control	max. Power / Windmill
	• Stab.	max. Power

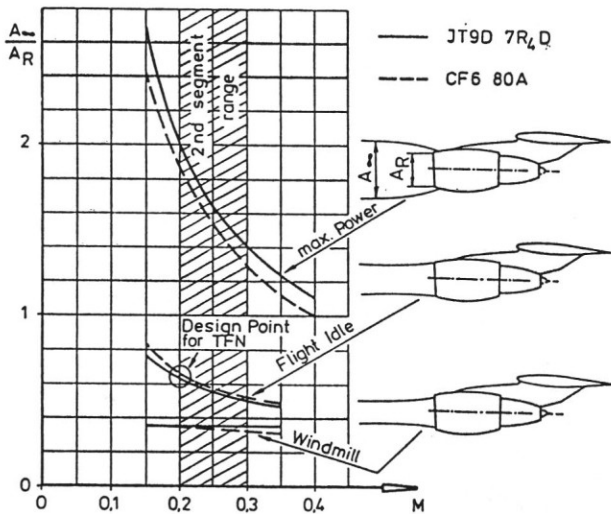


FIG. 5 Ratio of Free Stream Tube Area to Propulsion Highlight Area

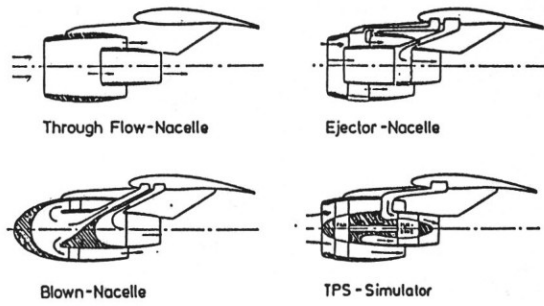


FIG. 6 Engine Simulation Concepts

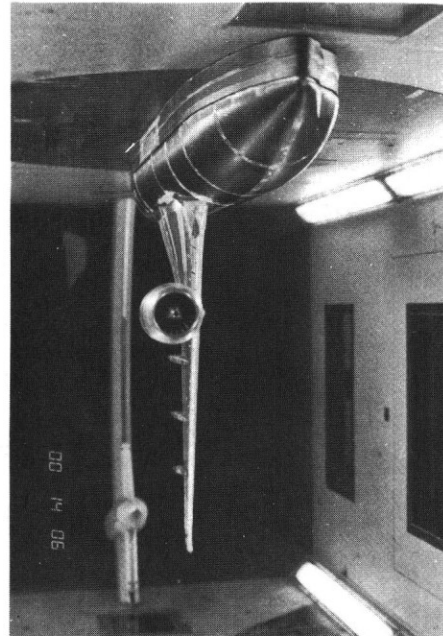


FIG. 7 A310 Half Model with TPS in the MBB Tunnel at Bremen

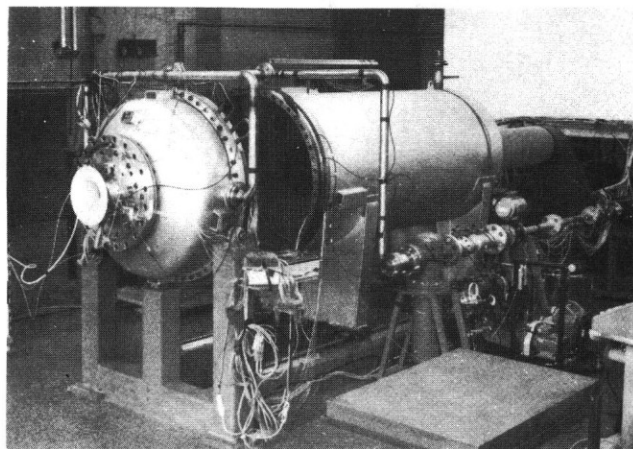


FIG. 8 MBB - TPS Calibration Tank

Wing in High Lift Configuration

FIG. 9

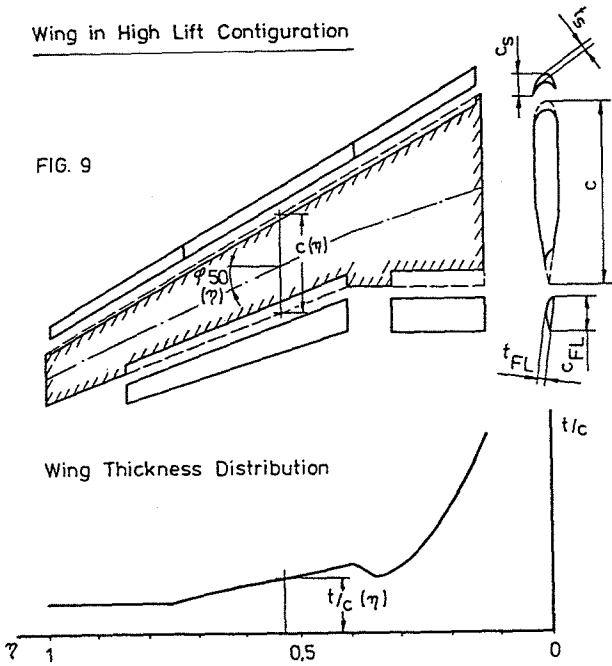


FIG. 9 Definition of Wing (Tailplane) Dimensions

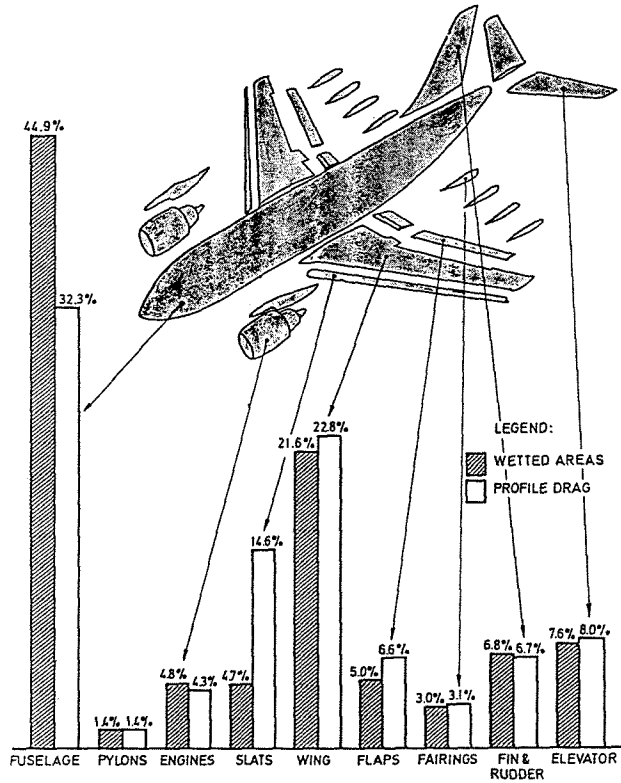


FIG. 12 Break-Down of Wetted Areas and Shape Drags A310

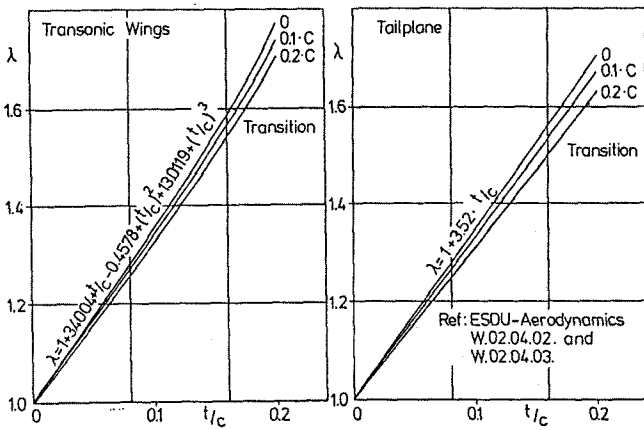


FIG. 10 Shape Factors for Wing and Tail Plane

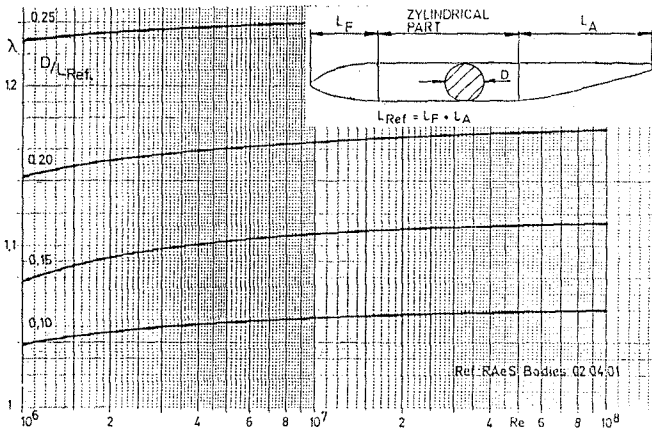


FIG. 11 Shape Factors for Fuselage

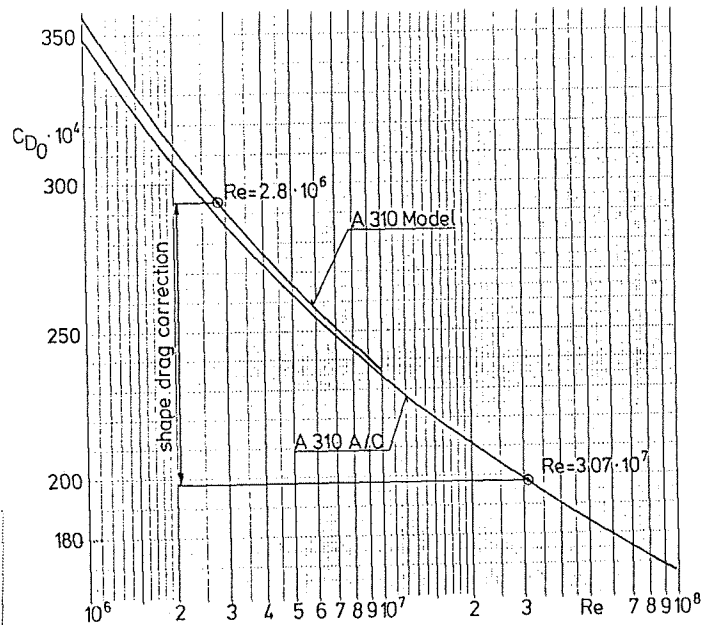


FIG. 13 Calculated Shape-Drags for A310 Model and Aircraft Conditions

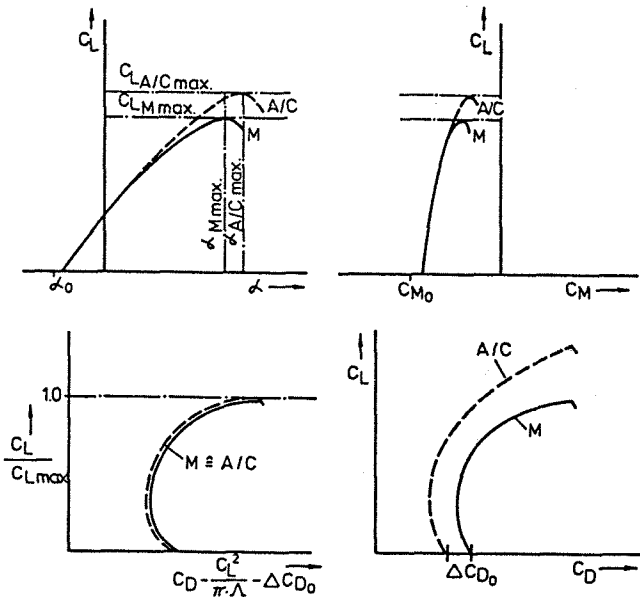


FIG. 14 Effect of Reynolds Number on Lift, Pitching Moment and Drag

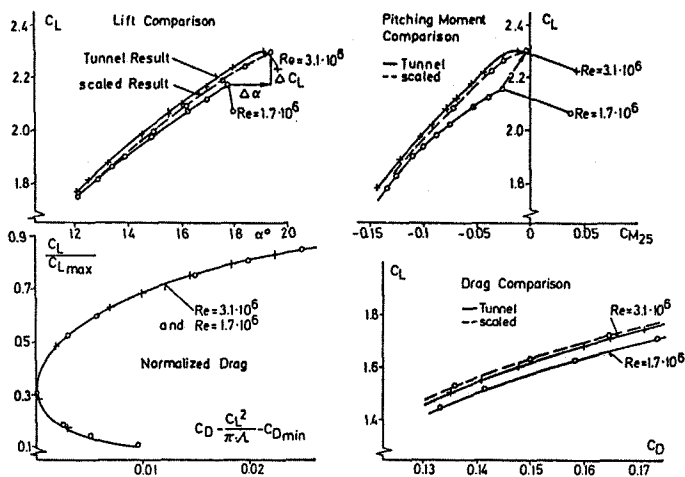


FIG. 15 Tunnel Results for  $R_N = 3.1 \times 10^6$  compared with Scaled Values based on Measurements at  $R_N = 1.7 \times 10^6$

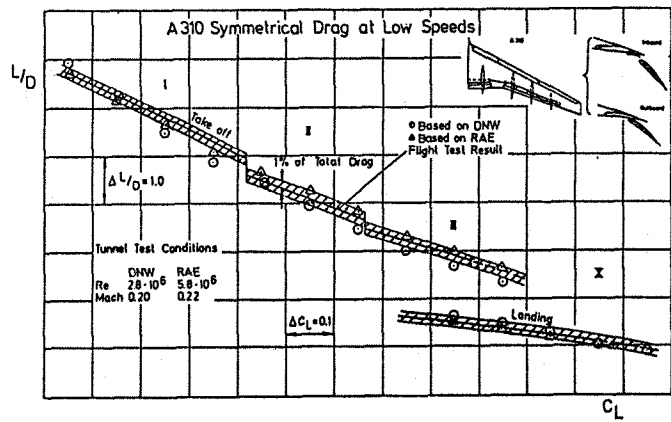


FIG. 16 Scaled Drags compared with Flight Test Results A310

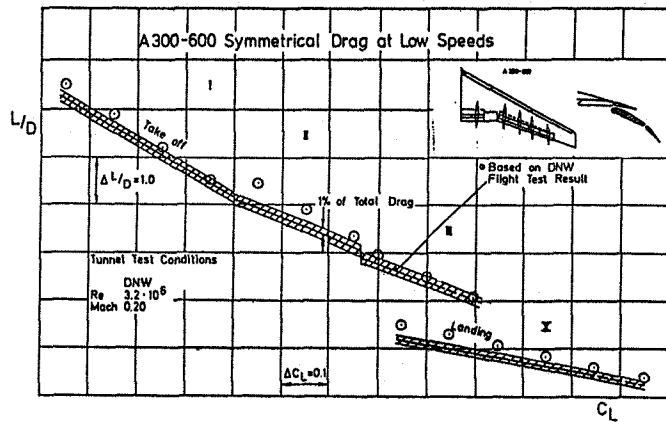


FIG. 17 Scaled Drags compared with Flight Test Results A300-600